Results in Physics 17 (2020) 103064

Contents lists available at ScienceDirect

Results in Physics

journal homepage: www.elsevier.com/locate/rinp

Investigation of continuum generation in the non-zero dispersion-shifted fiber pumped by femtosecond nanojoule pulses in 1450–1800 nm spectral range

Ieva Pipinytė[a,*], Julius Vengelis[a], Vygandas Jarutis[a], Mikas Vengris[a], Rimantas Grigonis[a], Valdas Sirutkaitis[a]

[a] Laser Research Center, Vilnius University, Sauletekio Ave. 10, Vilnius LT-10223, Lithuania

ARTICLE INFO

Keyword:
Fibers
Continuum generation
Femtosecond pulses
Nonlinear optics
Synchronously pumped optical parametric oscillator

ABSTRACT

A synchronously pumped optical parametric oscillator based on periodically poled potassium titanyl phosphate (PPKTP) crystal delivering femtosecond nanojoule energy pulses in the 1.45 μm–1.8 μm spectral range is used as pump source for continuum generation in conventional non-zero dispersion shifted optical fiber. Detailed numerical simulations and experiments employing cross-correlation frequency-resolved optical gating (XFROG) reveal soliton and dispersive wave generation dynamics and can help to estimate limits of how far the pump wavelength can be shifted from zero-dispersion wavelength (ZDW) to still obtain sufficient spectrum broadening. We also demonstrate the applicability of recently introduced fiber dispersion measurement technique based on XFROG trace analysis to conventional optical fibers. Combination of this efficient parametric device with standard non-zero dispersion shifted low cost and low loss optical fiber results in efficient continuum generation with output/input average power ratio greater than 50%.

Introduction

Extremely broadband spectrum generation, known as continuum (or supercontinuum) generation (CG), is a complex nonlinear optical phenomenon occurring during propagation of intense short laser pulses in various transparent media. Since its first observation in the borosilicate glass in 1970 [1] continuum generation quickly became a field of intense research [2]. At the same year the first continuum in bulk medium was demonstrated, researchers at *Corning* demonstrated a dramatic reduction of losses in optical fibers [3]. This immediately attracted interest for use of optical fibers not only for communications applications but also as nonlinear medium due to compactness, simplicity and robustness of such systems. First continuum generation in an optical fiber was observed in 1976 [4] by C. Lin and R. Stolen when they used 10 ns dye laser pulses pumping in the normal GVD (group velocity dispersion) range of conventional silica fiber to generate broadband continuum. During subsequent research by many groups it was realized that group velocity dispersion was the key factor determining CG in optical fibers, however, very few laser sources at that time were available to provide ultrashort pulses (down to a few picoseconds) with wavelengths close to zero dispersion wavelength (ZDW) of the optical fiber (i.e. ~ 1300 nm for conventional fused silica fibers) which would ensure most effective spectrum broadening [5,6]. At the same time (1990s) the need of developing wavelength division multiplexing systems [7–12] led to experiments where pumping around 1550 nm was utilized. Er-doped fiber lasers and amplifiers were among the first ultrashort laser systems with wavelengths around 1550 nm used for CG in conventional fused silica fibers [13–17].

The invention of photonic crystal fibers (PCFs) [18,19] was a major development in fiber optics. PCFs can have unique dispersive properties achieved by engineering geometry of their microstructured region [20] which was immediately used to shift ZDW of PCFs to the visible spectrum range where more efficient solid-state lasers were available as pump sources for CG [21–24]. Moreover, in PCFs light can be confined in a significantly smaller core resulting in enhanced nonlinearity which was applied to demonstrate continuum generation with very low (nanojoule) energy pump pulses [25,26]. Combined with fiber tapering technique, which enabled the reduction of conventional optical fiber core diameter [27,28], these technological innovations led to the fact that currently most CG experiments in optical fibers use tapered conventional fused silica fibers or PCFs (including tapered PCFs) [29–42].

In recent years, much attention is concentrated to CG in the near IR

* Corresponding author.
E-mail address: ieva.pipinyte@gmail.com (I. Pipinytė).

https://doi.org/10.1016/j.rinp.2020.103064
Received 30 January 2020; Received in revised form 10 March 2020; Accepted 14 March 2020
Available online 20 March 2020

and mid-IR spectral range due to its applicability in gas analysis, high resolution spectroscopy (numerous molecular absorption lines in mid-IR), optical coherence tomography (deeper tissue penetration in 2 μm–2.5 μm spectral range) and frequency metrology [43]. In case of femtosecond regime, setups of CG consisting of a Ti:sapphire laser as a pump source and PCF with ZDW close to 800 nm are considered as a standard for multi-octave continuum generation in the visible and near-IR spectral range[29]. Several femtosecond CG experiments in near and mid-infrared region were performed using other lasers (such as Cr:ZnS laser) and PCFs with two ZDWs [44], fibers made from fluoride or chalcogenide glass [45–48]. However, losses in such fibers are considerably greater than in standard fused silica fibers and the femtosecond pump lasers used in these experiments have limited wavelength tunability. There are also investigated special cases of varying dispersion influence for CG in diameter changing fibers using one pump wavelength [41,49,42]. Theoretical modeling of dynamical differences in CG due to pump wavelength tuning across ZDW is presented in [29]. Several experimental studies have investigated these dependencies experimentally [50,51], however the details allowing direct comparison between theory and experiment are still lacking. Recent advances in IR femtosecond synchronously pumped optical parametric oscillators (SPOPOs) have transformed them into efficient, compact and high beam quality devices delivering ultrashort pulses at high repetition rates tunable in a wide spectral range [52–54] present them as potential pump sources for IR continuum generation.

In this paper, we present a detailed experimental investigation of continuum generation in conventional non-zero dispersion shifted (NZDS) fiber pumped by femtosecond nanojoule energy pulses in the 1.45 μm–1.8 μm spectral range delivered by a synchronously pumped optical parametric oscillator (SPOPO) based on periodically poled potassium titanyl phosphate (PPKTP) crystal. Combination of this efficient parametric device [55,56] with standard low cost and low loss optical fiber result in efficient continuum generation with output/input average power ratio greater than 50%. Firstly, we used the SPOPO to continuously tune the wavelength of output pulses and investigated the CG at different pump wavelengths with a fixed peak power. By shifting pump wavelength from normal ($D < 0$, D – fiber dispersion parameter related to GVD as: $D = -\frac{2\pi c}{\lambda^2}\cdot GVD$) to anomalous ($D > 0$) dispersion region of our optical fiber we analyzed soliton and dispersive wave generation dynamics using XFROG technique. This revealed limits and peculiarities of how far the pump wavelength can be shifted from ZDW to still obtain sufficient spectrum broadening. Experimental results of continuum expansion obtained at different wavelengths and single peak power are accompanied with numerical simulation, which additionally revealed the alteration of the dispersion sign in normal dispersion region by intense soliton pulse from the anomalous dispersion region. Finally, we demonstrate the applicability of recently introduced fiber dispersion measurement technique [57] based on XFROG trace analysis to conventional optical fibers. This method was hirhertoo applied only for PCFs where extremely rapid spectrum expansion ensured high accuracy of dispersion estimation. We show that in conventional non-zero dispersion shifted fiber even with nanojoule pump pulses the condition of rapid spectrum expansion is valid and the method can be used for reliable estimation of fiber dispersion.

Materials and methods

Experimental setup

The experimental setup for PPKTP SPOPO and continuum generation in non-zero dispersion shifted fiber is shown in Fig. 1. The pump source for SPOPO was an Yb:KGW femtosecond laser oscillator generating 59 nJ energy 90 fs pulses with 76 MHz repetition rate at 1033 nm wavelength. The initial beam coming from the laser was split into two beams by a 1:1 energy ratio beamsplitter. One energy beam was used as pump for SPOPO, whereas the second energy beam was later used as a reference pulse for XFROG measurement. In contrast to the previously published SPOPO system [56], here we used a slightly different SPOPO configuration with 150 mm focal length lens and 27% output coupler transmittance.

The nonlinear medium for parametric generation was a 1 mm length periodically poled potassium titanyl phosphate crystal. The SPOPO cavity mirrors were highly reflecting for signal wave and enabled wavelength tuning from 1.45 μm to 1.8 μm. The tuning of output wavelength was achieved by changing SPOPO cavity length and using six different period crystal gratings: 33 μm, 34 μm, 35 μm, 36 μm, 37 μm and 38 μm. PPKTP SPOPO signal pulses characteristic at maximum pump intensity ($I_{pmax} \sim 40 GW/cm^2$, $P_{ave} = 2250$ mW) are depicted in Fig. 2.

For continuum generation we used a 4 m long non-zero dispersion-shifted optical fiber (*DCF4*, *Thorlabs*). The input coupling end of the fiber was mounted on the three axis translation stage (XYZ stage in the Fig. 1) and a 8 mm focal length aspheric lens was used to focus SPOPO radiation into the fiber. The dependence of continuum spectrum on the pump power was recorded by varing the fiber input power by attenuator and recording the spectra at the fiber output using NIR spectrometer (*Avantes AveSpec-NIR256-25*).

For investigation of CG, we used XFROG measurement technique, which apparatus is also included in Fig. 1. The generated continuum radiation and the reference beam were focused by a 101.6 mm focal distance aluminum parabolic mirror to a 600 μm thick beta barium borate (BBO) crystal cut at $\theta = 23°$ and $\phi = 90°$ type II phase matching. Using a fine tuning delay line we changed the time delay of the reference pulse with respect to the continuum pulse and recorded spectra of the corresponding sum-frequency signal produced by the interaction between continuum and reference pulses in the BBO crystal. Time resolution of the spectrogram was determined by the duration of reference pulse (≈ 90 fs), whereas the spectral resolution was determined by the spectrometer (1.3 nm).

Numerical simulation

The pulse in the fiber can be conveniently described by considering the electric field as the pulse envelope $\mathscr{E}$ with a carrier wave of frequency ω_0, i.e. $E(t, z) = \frac{1}{2}\mathscr{E}(t, z)e^{i\omega_0 t - ik_0 z} + c.c.$. In our model, the reference frequency ω_0 corresponds to the zero dispersion wavelength λ_0. Using the reference pulse frame $\zeta = z$, $\tau = t - z/v_g$, where v_g is the pulse group velocity at ω_0 and $k_0 = k(\omega_0)$ is the wave number of the fundamental fiber mode the electric field can be expressed as $E = \frac{1}{2}\mathscr{E}e^{i\omega_0(\tau+\zeta/v_g)-ik_0\zeta} + c.c.$. It is also convenient to use dimensionless pulse envelope amplitude A defined as $\mathscr{E} = \mathscr{E}_p A(\tau, \zeta)$, where $\mathscr{E}_p$ is the initial maximum amplitude of the pump pulse. Numerical simulations were performed using approximated nonlinear envelope equation, which can be written in the frequency domain as follows

$$\frac{\partial \hat{A}}{\partial \zeta} = \frac{k^2 - \kappa^2}{2i\kappa}\hat{A} + \frac{1}{2i\kappa}\frac{\omega^2}{c^2}\frac{\hat{P}_N}{\varepsilon_0}. \quad (1)$$

Here $\omega = \omega_0 + \Omega$, $\hat{A}(\Omega, \zeta)$ is the spectral amplitude of the pulse, $k = \omega n(\omega)/c$ is the wave number of the fundamental mode of the fiber, $\kappa = k_0 + \Omega/v_g$, and $\hat{P}_N/\varepsilon_0$ is the Fourier transform of $P_N/\varepsilon_0 = 2n_0 n_2 I_p A_N$ with nonlinear refractive index n_2, intensity $I_p = \frac{1}{2}\varepsilon_0 c n_p |\mathscr{E}_p|^2$ (n_p- refractive index for the pump), and the amplitude of nonlinear response

$$A_N = A(\tau, \zeta)\left((1-\alpha)|A(\tau, \zeta)|^2 + \alpha\int_{-\infty}^{\tau} R(\tau - \tau')|A(\tau', \zeta)|^2 d\tau'\right). \quad (2)$$

The first term of fraction $1 - \alpha$ represents an instantaneous Kerr response of the medium due to the electronic contribution to the polarization, while the second term describes a delayed component of fraction $\alpha = 0.18$, due to stimulated Raman scattering. The function $R(t)$ mimics the delayed response with a characteristic time $1/\Gamma = 32$ fs and frequency $\omega_R = 1/(12.2\text{ fs})$ [58]:

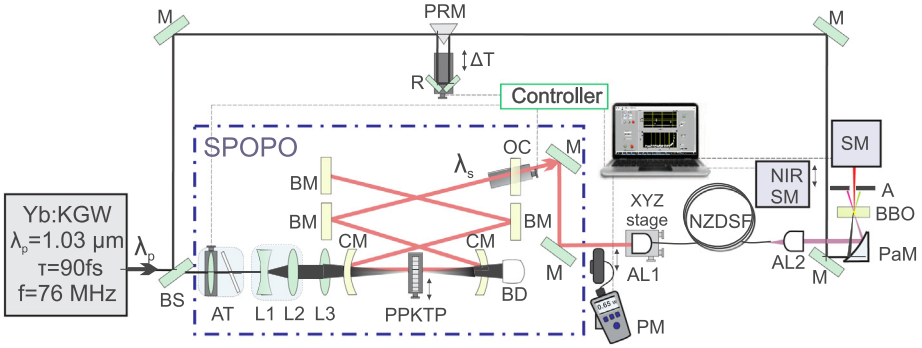

Fig. 1. Experimental setup of continuum generation in non-zero dispersion-shifted fiber and XGROG measurement apparatus: BS – beamsplitter, AT – attenuator consisting of $\lambda/2$ phase plate and Brewster type polarizer; L1, L2 – Galilean beam expander; L3 – focusing lens (f = 150 mm) for SPOPO pump radiation; CM – curved mirror; BD – beam dump; BM – broadband mirror; OC – output coupler; M – metal-coated mirror; PM – power meter; AL1 – coupling f = 8 mm aspheric lens; AL1 – collimating f = 11 mm aspheric lens; NZDSF– non-zero dispersion shifted optical fiber; NIR SM – infrared spectrometer, PaM – parabolic mirror, BBO – β- barium borate crystal, A – aperture, SM – spectrometer, PRM – prism mirror, R – retroreflector.

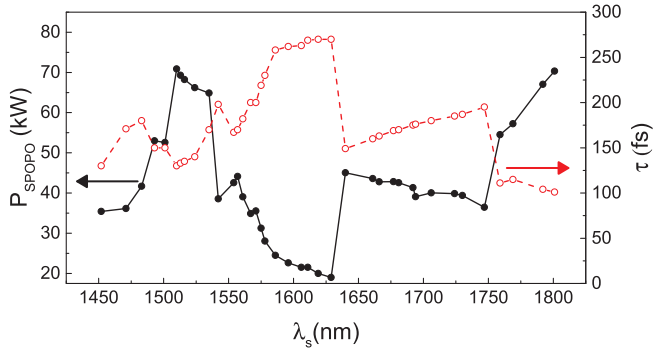

Fig. 2. SPOPO output characteristics: black line with filled circles – maximum peak power of SPOPO pulses, red dashed line with hollow circles – duration of SPOPO signal pulses.

$$R(t) = \frac{\Gamma^2 + \omega_R^2}{\omega_R} e^{-\Gamma t} \sin(\omega_R t). \tag{3}$$

In order to model different pumping frequencies ω_p, Eq. (1) was solved numerically using Gaussian pulses $A(\tau, 0) = \exp[-(\tau/\tau_p)^2 + i(\omega_p - \omega_0)\tau]$ with $\tau_p = 70$ fs.

The model Eq. (1) not only allows us to find the amplitude or spectra of the pulse propagating in the fiber, but also provides an estimate for the local effective dispersive parameter D_E. In order to explain how we calculate D_E it is convenient to rewrite the Eq. (1) in the form

$$\frac{\partial \hat{A}}{\partial \zeta} = -ik_L \hat{A} - ik_N \hat{F}, \tag{4}$$

where $k_L = (k^2 - \kappa^2)/(2\kappa)$ is the wave number of the wave (with frequency $\omega = \omega_0 + \Omega$) linearly propagating in the fiber, written in pulse frame of ZDW, $k_N = n_0 n_2 I_p \cdot (\omega/c)^2/\kappa$, and $\hat{F} = \hat{F}\{A_N\}$ represents Fourier transformation of A_N. Introducing real spectral amplitude and phase for pulse $\hat{A} = \hat{a}e^{i\hat{\phi}}$ and for the nonlinear response $\hat{F} = \hat{f}\, e^{i\hat{\psi}}$ one can deduce

$$-\frac{\partial \hat{\phi}}{\partial \zeta} = k_L + k_N \frac{\hat{b}}{\hat{a}} \equiv k_E, \tag{5}$$

here we denote $\hat{b} = \hat{f}\cos(\hat{\psi} - \hat{\phi})$. The coefficient k_E readily can be interpreted as the effective wave number and we can use it to find effective dispersive parameter D_E:

$$D_E = -\frac{2\pi c}{\lambda^2} \frac{\partial^2 k_E}{\partial \Omega^2} = D_L + D_N, \tag{6}$$

where $D_L = -2\pi c/\lambda^2 \cdot \partial^2 k_L/\partial\Omega^2$ represents ordinary dispersive parameter of the fiber, and D_N corresponds to induced dispersion due to nonlinearity of the medium. By differentiating the term $\hat{b}/\hat{a}$ with respect of Ω one obtain:

$$D_N = -\frac{2\pi c}{\lambda^2} k_N \frac{\hat{a}^2\hat{b}'' - \hat{a}(2\hat{a}'\hat{b}' + \hat{b}\hat{a}'') + 2\hat{b}(\hat{a}')^2}{\hat{a}^3}, \tag{7}$$

where $\hat{a}'$ and $\hat{b}'$ stand for derivatives of $\hat{a}$ and $\hat{b}$ with a respect of Ω. Although a numerator and a denominator of D_N can be calculated numerically from the known solution of Eq. (1), yet roundoff errors lead to very noisy results of D_N for spectral components where the numerator and the denominator approaches zero values. To overcome this issue we introduce numerically evaluable version of nonlinear dispersive coefficient, i.e. $\widetilde{D}_N = (\hat{a}/\hat{a}_{max})^3 D_N$, where $\hat{a}_{max}$ is the maximum spectral amplitude. With this choice we see that $\widetilde{D}_N \approx D_N$ where $\hat{a} \approx a_{max}$ and $\widetilde{D}_N \to 0$ when $\hat{a} \to 0$, i.e. where linear dispersion dominates. Therefore we define

$$\widetilde{D}_E = D_L + \left(\frac{\hat{a}}{\hat{a}_{max}}\right)^3 D_N \tag{8}$$

lThe numerically evaluable effective dispersive coefficient $\widetilde{D}_E$ has the same sign as the physical effective dispersive coefficient D_E for $\hat{a} \simeq \hat{a}_{max}$ and yet $\widetilde{D}_E$ approaches D_L for small spectral amplitudes $\hat{a}$. Thus the effective dispersive coefficient $\widetilde{D}_E$ can be used to explain some optical effects.

Results

Continuum broadening dependence on pump wavelength

The characteristics of the continuum generated at different pumping wavelengths and at maximum pump power are summarized in Fig. 3(a). Note that the real maximum peak power (P_p) used for continuum pump is ~47 % less than SPOPO output (P_{SPOPO}) due to the coupling losses. The maximum spectral broadening was obtained using pumping in the wavelength range of 1.49–1.62 μm. This corresponds to the normal dispersion and zero dispersion regions of the used fiber. The greatest obtained extension of spectrum (~34.5 THz) was at 1510 nm and 1513 nm continuum pump wavelengths, which corresponds to highest available peak power of SPOPO in normal dispersion area (Fig. 2). The widest spectrum (~400 nm) was obtained at 1510 nm and covers 1360–1760 nm spectral range (Fig. 3 b). It can be noticed that spectral broadening already starts at ~7 kW peak power which means that only 0.9 nJ pulse energy is needed for the spectral modulation to start.

Summarized experimental and theoretical simulation results of the spectral broadening at different pump wavelengths are presented in Fig. 4(a). At first glance, two humps can be noticed in Fig. 4 and their peaks, which denote biggest extension of continuum in each case, are separated by ~100 nm in the case of P_p = 10 kW. Moreover the position

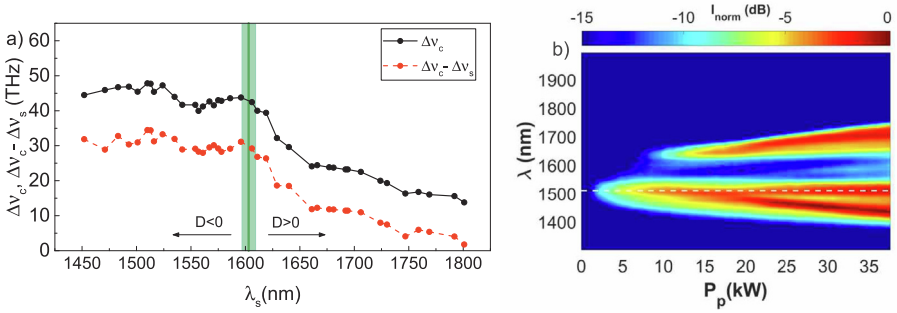

Fig. 3. (a) Continuum width ($\Delta\nu_c$) and width differences of continuum and signal ($\Delta\nu_c$- $\Delta\nu_s$) measured at −20 dB power level at maximum peak power (P_p). The green line and area indicates the estimated ZDW and its uncertainty level. (b) The spectra of continuum generated at 1510 nm wavelength presented as a function of pump power.

of the first peak, which is father from ZDW (marked in graphs as B), slightly changes depending on the pump peak power: at lower P_p it moves to a longer wavelength. Comparing the experimental results, the point B at P_p = 10 kW from 1483 nm moves to 1493 nm (B′) when P_p = 4 kW. This trend in theoretical curves shown as dashed red line: B_t at P_p = 13 kW is at 1470 nm and at P_p = 5 kW it corresponds to 1510 nm.

For better comparison we extracted experimental and theoretical spectral widths of continuum in the case of P_p = 10 kW pump power and presented in Fig. 5. Here we distinguished six characteristic points (they are marked in Fig. 5 by capital letters). It should be noted that positions of experimental (D_e) and theoretical (D_t) points slightly differ, but for the simplicity we will continue to use only D without any index. The experimental spectra of corresponding continua are presented in the first column of Fig. 6. The second and third columns of Fig. 6 also show the experimental dependencies of CG on the input power and the XFROG traces of the continua. It should be mentioned that XFROG traces were measured at different peak powers. The 13 kW peak power was used in the case of 1586 nm wavelength, because it corresponded to the maximum achievable peak power at this wavelength. Unfortunately, in the case of other pump wavelengths at this peak power SPOPO stability was lower (due to working near the threshold of the parametric generation or some slight misalignment of the resonator). For this reason, we chose 16 kW as the peak power at which most of discussed points could be measured in the stable mode. XFROG traces of corresponding continuua from the numerical modeling, are shown in Fig. 7. A, C and E points mark areas of reduced spectrum broadening efficiency and from 1724 nm to the point F the narrowing of spectral width is observed. We have to mentioned that some disagreement can be noticed comparing experimental and numerical XFROG traces in the anomalous dispersion area. However, we believe that the model used in our calculations is quite adequate to reality [59] and certainly can reproduce the solitonic waves as can be clearly seen in Fig. 7 (D-F). The observed discrepancy most likely is related to a refractive index of the fundamental mode, which was used in numerical modeling. Unfortunately we do not know a $n_{core}(\omega)$ and a $n_{cladding}(\omega)$ of the fiber and

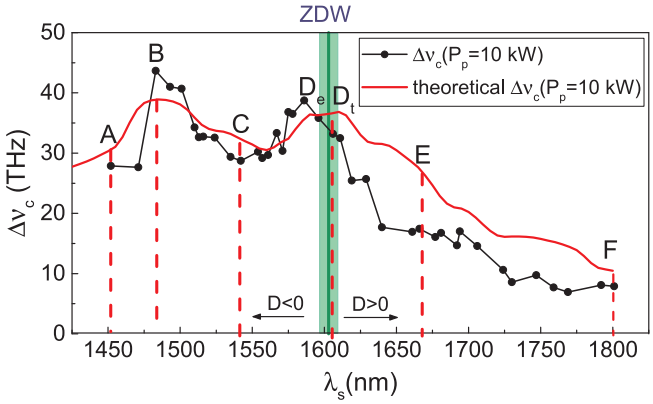

Fig. 5. Experimental and theoretically estimated continuum width ($\Delta\nu_c$) at P_p = 10 kW. The green line and area indicate the estimated ZDW and its uncertainty level.

therefore cannot simulate the accurate $n_{mode}(\omega)$, which is the crucial parameter in such calculations. In order to get reasonable values of the $n_{mode}(\omega)$ we used refractive index formula of silica glass for the $n_{core}(\omega)$ and adjusted the difference $n_{core} - n_{cladding}$ to reproduce experimentally measured dispersive coefficient D as much as it was possible. The dispersive coefficient D most accurately can be determined near ZDW. Hence, we think that is the main reason for the decreased agreement between calculated and experimental XFROG traces farther away from ZDW.

It is easy to see that numerically calculated spectral widths of output radiation qualitatively match the experimentally registered ones in terms of central wavelengths of the pump pulses. Our calculations reveal that positions of the peak B depend essentially on the magnitude of nonlinearity $n_2 I_p$. It is worth to note that the commonly accepted value of nonlinear index for silica fibers, i.e. $n_2 = 2.6 \cdot 10^{-8}$ μm²/W. In combination with this value, the effective mode diameter (A_{eff}), provided

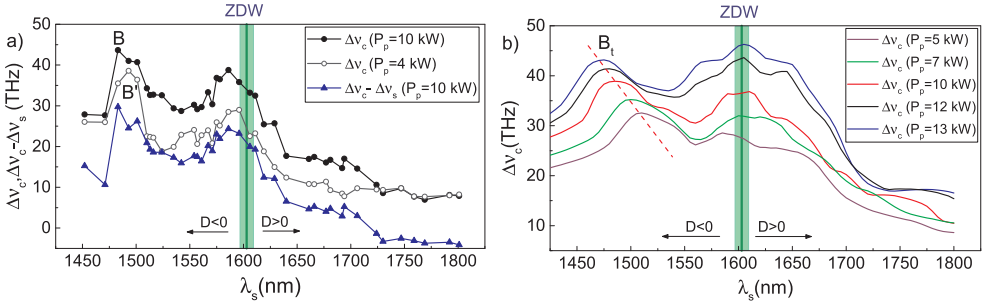

Fig. 4. (a) Continuum width ($\Delta\nu_c$) measured at −20 dB power level at P_p = 10 kW and P_p = 4 kW (a), width differences of continuum and signal ($\Delta\nu_c$- $\Delta\nu_s$) at P_p = 10 kW. (b) theoretically estimated continuum width at various P_p values. The green line and area indicate the estimated ZDW and its uncertainty level.

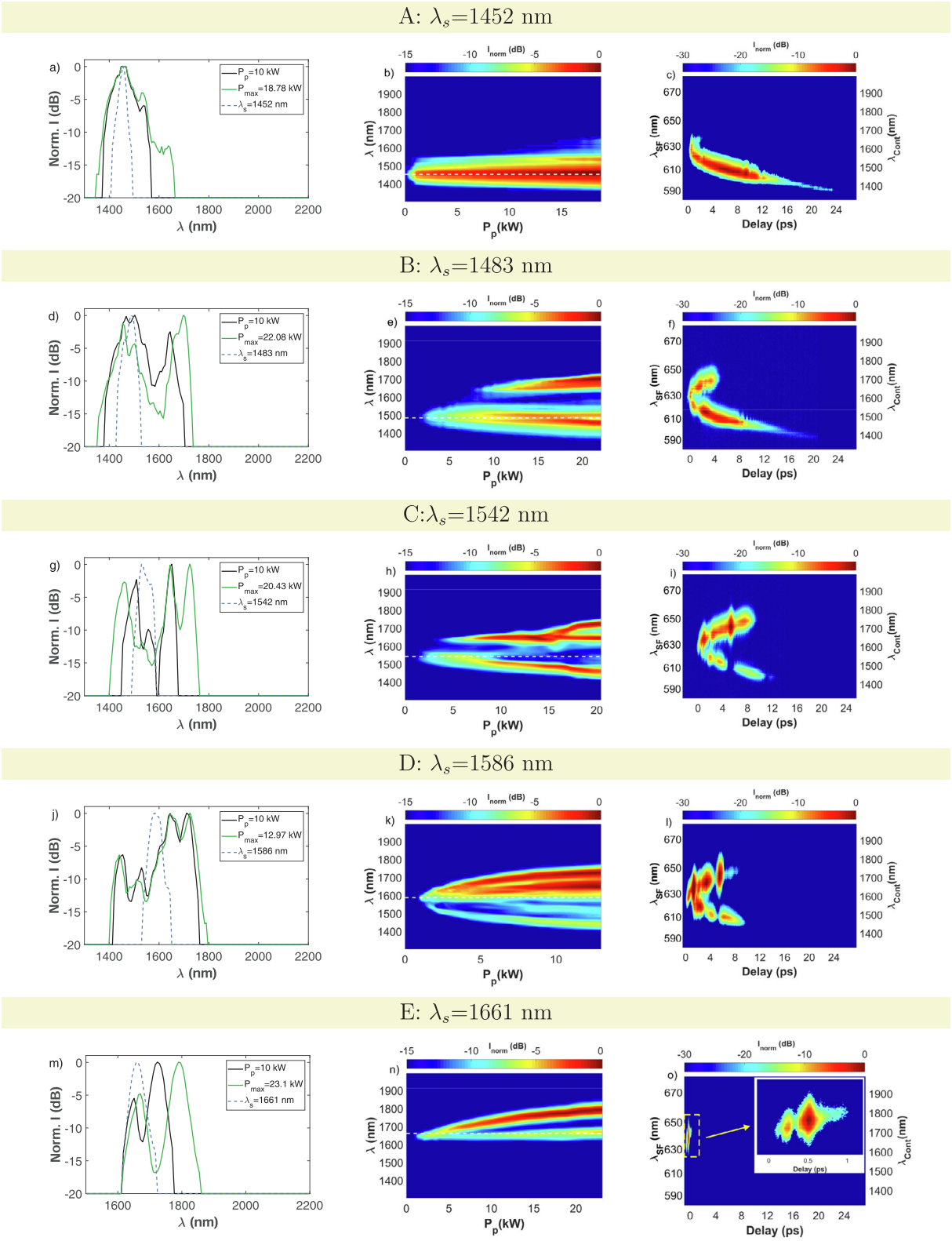

Fig. 6. Discrete spectra (a, d, g, j, m) at maximum P_p(green line), P_p = 10 kW (black line) and SPOPO signal spectra (dashed blue line) used for the continuum pump. Corresponding colormaps of continuum spectra (b, e, h, k, n) and XFROG traces at P_p = 16 kW (c, f, i, o) and at P_p = 13 kW (l). Note, that in case of λ_s = 1586 nm, the peak power of P_p = 13 kW was the highest achievable pump peak power.

by fiber suppliers, and experimental value of peak power, we were forced to increase the value of $n_2 I_p$ by a factor of 3 to obtain agreement between calculations and experimental results. The most plausible explanation for such discrepancy is the possibility that the effective diameter of the fundamental mode propagating inside the fiber is reduced by factor $\sqrt{3}$ due to nonlinear self-modulation and effective mode area could be significantly smaller than specified by fiber supplier. It is also interesting that other pump pulse parameters such as pulse width

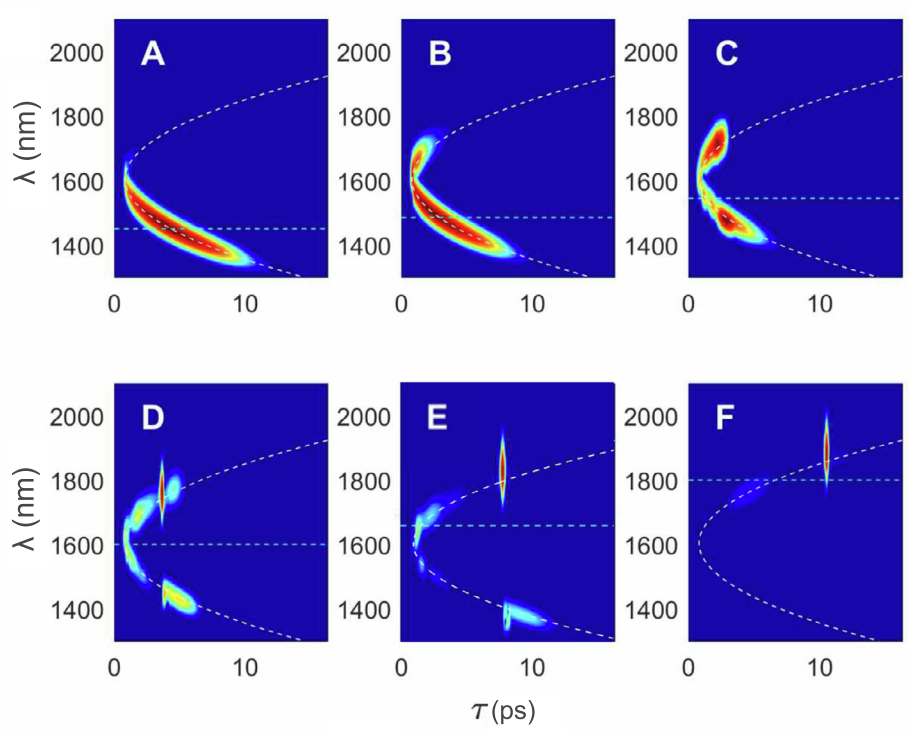

Fig. 7. Numerical simulated XFROG traces at $P_p = 10$ kW at corresponding pump wavelengths (dashed horizontal line): A (1450 nm), B(1485 nm), C(1540 nm), D (1605 nm), E(1665 nm), F(1800 nm).

or chirp have surprisingly weak impact on these peak positions. We think that observed phenomena depends on how far pump wavelength is from ZDW and how quickly the spreading of spectrum takes place, which of course depends on pump power and nonlinear index of refraction. Such behaviour will be discussed in more details in the "Discussion" section.

Estimation of fiber dispersion

For the estimation of our fiber's dispersion, we employed the method suggested for photonic crystal fibers in Ref.[57], which is based on the interplay between linear and nonlinear effects during CG. In order to make reliable estimations, the condition of the rapid spectrum broadening, when almost all continuum spectral components are created at the same time, has to be fulfilled. This rapid expansion of our case is demonstrated by simulated continuum evolution in Fig. 8. In Ref.[57], it was shown that since XFROG traces contain information about relative delay (τ) between continuum spectral components and the reference component (in our case $\lambda = 1.03$ μm), the dispersion of fiber can be estimated from:

$$D = \frac{1}{L}\frac{d\tau}{d\lambda}, \tag{9}$$

here L - continuum propagation distance (fiber length). And the uncertainty of dispersion:

$$\delta D = 2\sqrt{(D\delta L/L)^2 + (\delta(\tau'_\lambda)/L)^2}. \tag{10}$$

Following these expressions, we determined the dispersion of our fiber from seven XFROG measurements. Two results of these measurements (one in case of non-solitonic continuum extention mode (a, c) and other in solitonic mode (b, d)) are shown in Fig. 9. Despite the fact that dispersion estimation results are in good agreement in both cases, non - solitonic mode produces the data that requires less point elimination before fitting the disperssion to a polynomial. This is related to the fact that the delay function in the anomalous dispersion

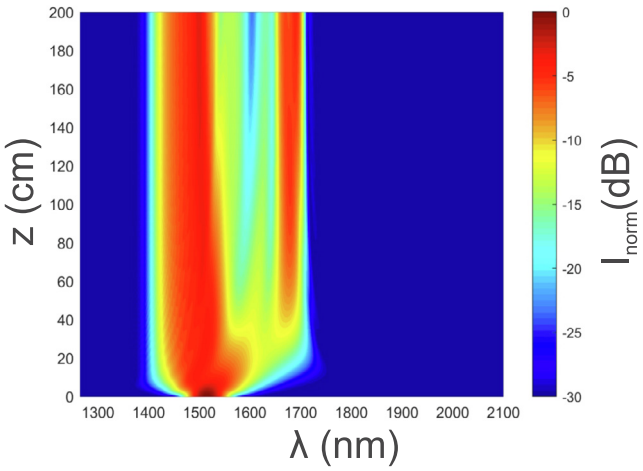

Fig. 8. Numerically simulated evolution of the continuum in NZDS fiber. Pump wavelength is $\lambda_s = 1516$ nm, peak power $P_p = 10$ kW.

region is more complex, because several delays corresponds not to one but many wavelengths. At such cases, we have chosen the wavelength, which is most correlated with the closest delay which does not have this ambiguity, assuming that dispersion does not have steep leaps. Our calculated average ZDW was equal to 1603 ± 6 nm. The supplier of the fiber provides not ZDW point, but D = −4 $ps/nm{\cdot}km$ at 1550 nm wavelength. We obtained D = $-8 \pm 4 ps/nm{\cdot}km$, which is in a good agreement (within the margin of errors) with the data provided by suppliers and shows the reliability of this method for dispersion measurement of conventional fibers.

Discussion of continuum evolution dynamics in terms of pump wavelength

In this section, our objective is to discuss the obtained dependency

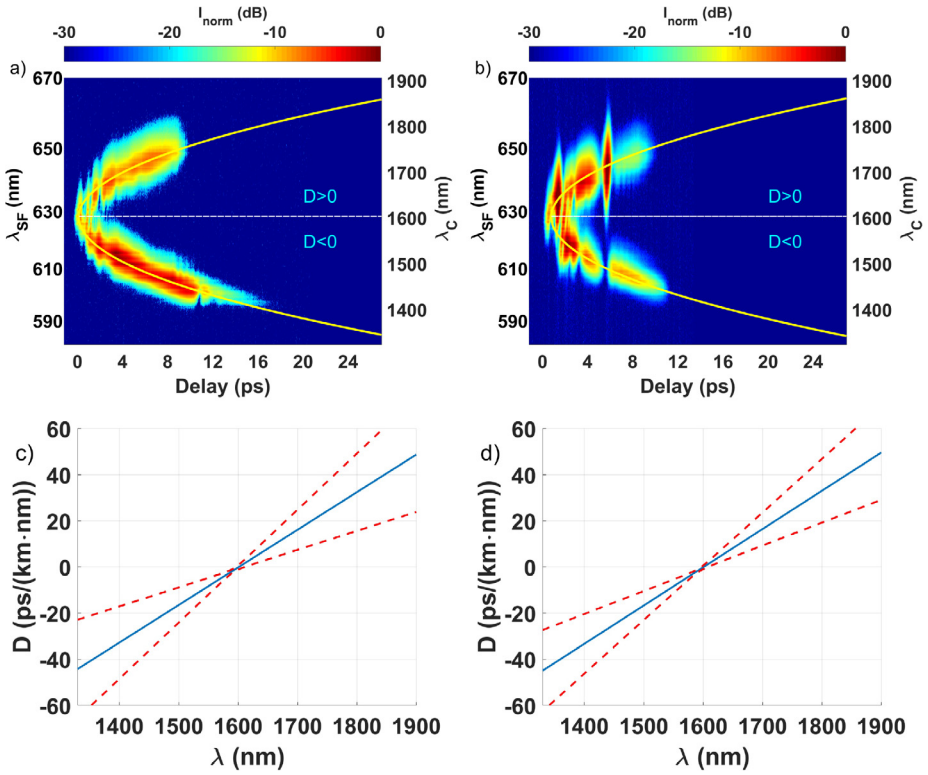

Fig. 9. (a, b) Measured XFROG traces with fitted polynomial curves. Dashed white line indicates ZDW. (c, d) Calculated dispersion of NZDS fiber (solid blue line). Red dashed lines indicate uncertainty interval at confidence level of 95 %. Results obtained at: (a,c) $\lambda_s = 1516$ nm, $P_p = 36$ kW and (b,d) $\lambda_s = 1567$ nm, $P_p = 18.5$ kW.

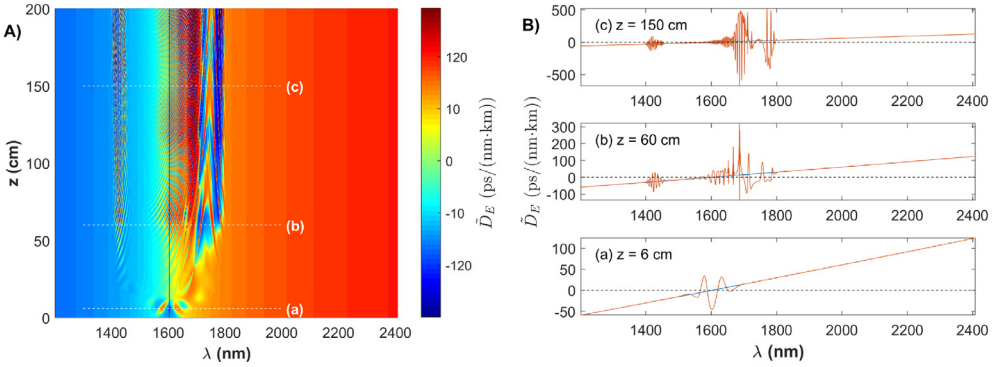

Fig. 10. (A) Numerically simulated evolution of dispersive parameter ($\tilde{D}_E$) using pulse propagation in NZDS fiber; (B) Numerical simulated dispersive parameter at certain fiber lengths. Pump wavelength: $\lambda_s = 1605$ nm.

of continuum characteristics on pump wavelength and the underlying causes. Experimental and numerical simulation results (Fig. 4(b)) exhibit the same tendency of continuum behavior: both curves have two humps, i.e. the positions where widest extension of spectrum is obtained and the spectral intervals between them are similar. Moreover, both results show decreasing of spectral broadening at pump wavelengths corresponding to the anomalous dispersion area. In order to understand such behavior, we presented XFROG traces (Fig. 7) at characteristic points marked on the curve in Fig. 5. The point A corresponds to the case, where the entire pump spectrum is in the normal dispersion (D < 0) range and the main mechanism causing the broadening is self phase modulation (SPM). This result is similar to the results of numerical simulations of CG in photonic crystal fibers in [29]. Here, the SPM leads to almost negligible energy transfer to the anomalous dispersion range. At point B (which is a little bit closer to ZDW) the SPM is still dominant cause of spectral broadening, but differs from the case of A, in that more energy gets transferred to the anomalous (D > 0) zone. The redistribution of energy during this process reduces the peak power and soliton still has no chance of being formed. At this point, we obtain the widest continuum spectrum, and since this is still non-solitonic spreading, the obtained spectrum retains continuous phase relationships between different frequencies that allow effective pulse compression [60]. As we mentioned earlier, the position of point B depends on pump peak power (Fig. 4). This is related to the fact, that at higher peak powers energy from shorter wavelengths can be transferred to the anomalous dispersion range. At point C (even closer to ZDW), even more energy is relocated to the anomalous dispersion range, and mixed normal dispersion and soliton mode is observed [29]. At certain time instances, we observe radiation at both branches of the dispersion curve. The interaction between them can occur via cross phase modulation (XPM) [29,61] and four - wave mixing (FWM) [31,61,41]. Due to the fact that all these processes (together with soliton formation and SPM) are dependent on peak power, they are weakened during propagation and this limits the formation of new spectral components [49]. The point D likely matches the condition where pulse trapping occurs: the soliton in anomalous dispersion and trapped pulse in normal

dispersion regimes overlap in time scale and copropagate along the fiber [62,42]. Numerical simulation results show the effective dispersion parameter modulations, which occur during propagation of intense pulse in the fiber (Fig. 10). It can be noticed that at ~1425 nm wavelength (see Fig. 10 B (b) and (c) cases) these modulations cross the zero value of the dispersion parameter. Here soliton (an intense pulse in anomalous dispersion area) alters the local dispersion sign in normal dispersion region causing the formation of trapped waves. Thus, the resulting trapped wave can be described as a dispersive wave propagating in the spectral range of normal dispersion ($D_L < 0$) with local effective dispersion ($D_E > 0$) induced by a soliton. Further increase of pump wavelength (point E and F) corresponds to soliton-dominant continuum. Here the energy exchange between opposite dispersion regions is diminished and the spectral width is mainly determined by the formation of soliton spectra. In contrast to earlier work [29], we did not observe the tendency of pump wavelengths in anomalous dispersion range to produce wider spectra. This most probably is related to the fact that the previous work investigated a photonic crystal fiber, hence the spectrum broadening was caused by higher nonlinearity than conventional fiber investigated here.

Conclusion

We have presented experimental investigation and numerical simulations of continuum generated in non-zero dispersion-shifted fiber by the femtosecond pulses produced by synchronously pumped optical parametric oscillator (in the 1.45–1.8 μm spectral range). The results show that the most effective continuum generation can be obtained at two pump wavelengths, these points are separated by each other by ~100 nm at $P_p = 10$ kW and produce different types of continuum: non-solitonic and solitonic. Moreover, the experimental and theoretical results show that the position of the point, which corresponds to non-solitonic continuum, depends on pump intensity and fiber nonlinearity. To sum it up, the most effective continuum of the non-solitonic mode, which has advantages in applications of pulse compression or dispersion measurements, in a particular fiber with a given nonlinear refractive index can be obtained at smaller pump wavelength using higher pump power. Moreover, numerical estimation of local dispersion parameter shows that an intense soliton formed in the spectral range with anomalous dispersion can modulate the local dispersion in the spectral range with normal dispersion, resulting in the formation of trapped waves. Finally, we demonstrate that in a conventional non-zero dispersion-shifted fiber pumped at nanojoule pump pulses, the rapid continuum expansion condition is valid and fiber dispersion can be reliably measured using XFROG based method of Ref. [57].

CRediT authorship contribution statement

Ieva Pipinytė: Conceptualization, Investigation, Writing - original draft, Visualization. **Julius Vengelis:** Methodology, Writing - review & editing. **Vygandas Jarutis:** Software, Formal analysis, Writing - original draft, Visualization. **Mikas Vengris:** Writing - review & editing. **Rimantas Grigonis:** Resources, Supervision. **Valdas Sirutkaitis:** Resources, Supervision.

Declaration of Competing Interest

The authors declare that they have no known competing financial interests or personal relationships that could have appeared to influence the work reported in this paper.

Acknowledgments

This research is funded by the European Social Fund according to the activity 'Improvement of researchers' qualification by implementing world-class R&D projects' of Measure No. 09.3.3-LMT-K-712, Grant No. 09.3.3–712-0014.

References

[1] Alfano RR, Shapiro S. Emission in the region 4000 to 7000 Åvia four-photon coupling in glass. Phys Rev Lett 1970;24(11):584–7. https://doi.org/10.1103/PhysRevLett.24.584.
[2] R.R., The supercontinuum laser source, Springer, 2006.
[3] Kapron FP, Keck DB, Maurer RD. Radiation losses in glass optical waveguides. Appl Phys Lett 1970;17(10):423–5. https://doi.org/10.1063/1.1653255.
[4] Lin C, Stolen RH. New nanosecond continuum for excited-state spectroscopy. Appl Phys Lett 1976;28(4):216–8. https://doi.org/10.1063/1.88702.
[5] Kodama Y, Hasegawa A. Monlinear pulse propagation in a monomode dielectric guide. IEEE J Quantum Electron. 1987;23(5):510–24. https://doi.org/10.1109/JQE.1987.1073392.
[6] Islam MN, Sucha G, Bar-Joseph I, Wegener M, Gordon JP, Chemla DS. Broad bandwidths from frequency-shifting solitons in fibers. Opt Lett 1989;14(7):370–2. https://doi.org/10.1364/OL.14.000370.
[7] Morioka T, Mori K, Saruwatari M. More than 100-wavelength-channel picosecond optical pulse generation from single laser source using supercontinuum in optical fibres. Electron Lett 1993;29(10):862–4. https://doi.org/10.1049/el:19930576.
[8] Takara H, Kawanishi S, Morioka T, Mori K, Saruwatari M. 100 Gbit/s optical waveform measurement with 0.6ps resolution optical sampling using subpicosecond supercontinuum pulses. Electron Lett 1994;30(14):1152–3. https://doi.org/10.1049/el: 19940796.
[9] Morioka T, Kawanishi S, Mori K, Saruwatari M. Transform-limited, femtosecond WDM pulse generation by spectral filtering of gigahertz supercontinuum. Electron Lett 1994;30(14):1166–8. https://doi.org/10.1049/el:19940805.
[10] Morioka T, Kawanishi S, Mori K, Saruwatari M. Nearly penalty-free, < 4 ps supercontinuum Gbit/s pulse generation over 1535–1560 nm. Electron Lett 1994;30(10):790–1. https://doi.org/10.1049/el:19940520.
[11] Kawanishi S, Takara H, Morioka T, Kamatani O, Saruwatari M. 200 Gbit/s and 100 km time-division-multiplexed optical-transmission using supercontinuum pulses with prescaled PLL timing extraction and all-optical demultiplexing. Electron Lett 1995;31(10):816–7. https://doi.org/10.1049/el:19950569.
[12] Mikulla B, Leng L, Sears S, Collings BC, Arend M, Bergman K. Broad-band high-repetition-rate source for spectrally sliced WDM. IEEE Photonics Technol Lett 1999;11(4):418–20. https://doi.org/10.1109/68.752534.
[13] Okuno T, Onishi M, Nishimura M. Generation of ultra-broad-band supercontinuum by dispersion-flattened and decreasing fiber. IEEE Photonics Technol Lett 1998;10(1):72–4. https://doi.org/10.1109/68.651109.
[14] Mori K, Takara H, Kawanishi S. Analysis and design of supercontinuum pulse generation in a single-mode optical fiber. J Opt Soc Am B 2001;18(12):1780–92. https://doi.org/10.1364/JOSAB.18.001780.
[15] Nishizawa N, Goto T. Widely broadened super continuum generation using highly nonlinear dispersion shifted fibers and femtosecond fiber laser. JJAP 2001;40(Part 2, No. 4B):L365–7. https://doi.org/10.1143/jjap.40.l365.
[16] Gu Y, Zhan L, Deng D, Wang Y, Xia Y. Supercontinuum generation in short dispersion-shifted fiber by a femtosecond fiber laser. Laser Phys. 2010;20:1459–62. https://doi.org/10.1134/S1054660X1011006X.
[17] Moon S, Kim DY. Generation of octave-spanning supercontinuum with 1550-nm amplified diode-laser pulses and a dispersion-shifted fiber. Opt Express 2006;14(1):270–8. https://doi.org/10.1364/OPEX.14.000270.
[18] Knight JC, Birks TA, Russell PSJ, Atkin DM. All-silica single-mode optical fiber with photonic crystal cladding. Opt Lett 1996;21(19):1547–9. https://doi.org/10.1364/OL.22.000484.
[19] Cregan RF, Mangan BJ, Knight JC, Birks TA, Russell PSJ, Roberts P, Allan DC. Single-mode photonic band gap guidance of light in air. Science 1999;285:1537–9. https://doi.org/10.1126/science.285.5433.1537.
[20] Saitoh K, Koshiba M. Empirical relations for simple design of photonic crystal fibers. Opt Express 2005;13(1):267–74. https://doi.org/10.1364/OPEX.13.000267. arXiv:arXiv:0809.2388v1.
[21] Knight JC, Arriaga J, Birks TA, Wadsworth WJ, Russell PSJ. Anomalous dispersion in photonic crystal fiber. IEEE Photonics Technol Lett 2000;12(7):807–9. https://doi.org/10.1109/68.853507.
[22] Reeves WH, Skryabin DV, Biancalana F, Knight JC, Russell PSJ, Omenetto FG, Efimov A, Taylor AJ. Transformation and control of ultra-short pulses in dispersion-engineered photonic crystal fibres. Nature 2003;424:511–5. https://doi.org/10.1038/nature01798.
[23] Mogilevtsev D, Birks TA, Russell PSJ. Group-velocity dispersion in photonic crystal fibers. Opt Lett 1998;23(21):1662–4. https://doi.org/10.1364/OL.23.001662.
[24] Ranka JK, Windeler RS, Stentz AJ. Optical properties of high-delta air silica microstructure optical fibers. Opt Lett 2000;25(11):796–8. https://doi.org/10.1364/OL.25.000796.
[25] Ranka JK, Windeler RS, Stentz AJ. Visible continuum generation in air–silica microstructure optical fibers with anomalous dispersion at 800 nm. Opt Lett 2000;25(1):25–7. https://doi.org/10.1364/OL.25.000025.
[26] Wadsworth WJ, Ortigosa-Blanch A, Knight JC, Birks TA, Man T-PM, Russell PSJ. Supercontinuum generation in photonic crystal fibers and optical fiber tapers: a novel light source. J Opt Soc Am B 2002;19(9):2148–55. https://doi.org/10.1364/JOSAB.19.002148.
[27] Birks TA, Wadsworth WJ, Russell PSJ. Supercontinuum generation in tapered fibers. Opt Lett 2000;25(19):1415–7. https://doi.org/10.1364/OL.25.001415.

[28] Wadsworth WJ, Ortigosa-Blanch A, Knight JC, Birks TA, Man T-PM, Russell PSJ. Supercontinuum generation in photonic crystal fibers and optical fiber tapers: a novel light source. J Opt Soc Am B 2002;19(9):2148–55. https://doi.org/10.1364/JOSAB.19.002148.
[29] Dudley JM, Genty G, Coen S. Supercontinuum generation in photonic crystal fiber. Rev Mod Phys 2006;78(4):1135–84. https://doi.org/10.1103/RevModPhys.78.1135.
[30] Gu X, Kimmel M, Shreenath AP, Trebino R, Dudley JM, Coen S, Windeler RS. Experimental studies of the coherence of microstructure-fiber supercontinuum. Opt Express 2003;11(21):2697–703. https://doi.org/10.1364/OE.11.002697.
[31] Gorbach A, Skryabin D, Stone J, Knight J. Four-wave mixing of solitons with radiation and quasi-nondispersive wave packets at the short-wavelength edge of a supercontinuum. Opt Express 2006;14(21):9854–63. https://doi.org/10.1364/OE.14.009854.
[32] Liu X, Xu C, Knox WH, Chandalia JK, Eggleton BJ, Kosinski SG, Windeler RS. Soliton self-frequency shift in a short tapered air–silica microstructure fiber. Opt Lett 2001;26(6):358–60. https://doi.org/10.1364/OL.26.000358.
[33] Herrmann J, Griebner U, Zhavoronkov N, Husakou A, Nickel D, Knight JC, Wadsworth WJ, Russell PSJ, Korn G. Experimental evidence for supercontinuum generation by fission of higher-order solitons in photonic fibers. Phys Rev Lett 2002;88:173901 https://doi.org/10.1103/PhysRevLett.88.173901.
[34] Genty G, Lehtonen M, Ludvigsen H, Kaivola M. Enhanced bandwidth of supercontinuum generated in microstructured fibers. Opt Express 2004;12(15):3471–80. https://doi.org/10.1364/OPEX.12.003471.
[35] Kudlinski A, Cumberland B, Travers J, Bouwmans G, Quiquempois Y, Mussot A. CW supercontinuum generation in photonic crystal fibres with two zero-dispersion wavelengths. AIP Conf. Proc. 2008;1055:15–8. https://doi.org/10.1063/1.3002529.
[36] Bugar I, Fedotov IV, Fedotov AB, Koys M, Buczynski R, Pysz D, Chlpik J, Uherek F, Zheltikov AM. Polarization-controlled dispersive wave redirection in dual-core photonic crystal fiber. Laser Phys 2008;18(12):1420–8. https://doi.org/10.1134/S1054660X08120086.
[37] Qi X, Chen S, Liu T, Hou J. Enhanced visible supercontinuum generation in seven-core photonic crystal fiber. Proc. SPIE 2016;10016. https://doi.org/10.1117/12.2246309. 100160C–1–6.
[38] Klimczak M, Komolibus K, Piwoński T, Siwicki B, Pysz D, Stepień R, Ochalski T, Buczyński R. Impact of steepness of pump temporal pulse profile on spectral flatness and correlation of supercontinuum in all-solid photonic crystal fibers with flattened normal dispersion. J Opt 2014;16:1–9. https://doi.org/10.1088/2040-8978/16/8/085202.
[39] Siwicki B, Klimczak M, Sobon G, Sotor J, Pysz D, Stepien R, et al. Numerical simulations of spectral broadening in all-normal dispersion photonic crystal fiber at various pump pulse conditions. Opt Eng 2015;54(1). https://doi.org/10.1117/1.OE.54.1.016102. 016102–1–8.
[40] Vengelis J, Jarutis V, Sirutkaitis V. Extension of supercontinuum spectrum, generated in polarization-maintaining photonic crystal fiber, using chirped femtosecond pulses. Opt Eng 2018;57(1):1–10. https://doi.org/10.1117/1.OE.57.1.016102.
[41] Bendahmane A, Braud F, Conforti M, Barviau B, Mussot A, Kudlinski A. Dynamics of cascaded resonant radiations in a dispersion-varying optical fiber. Optica 2014;1(4):243–9. https://doi.org/10.1364/OPTICA.1.000243.
[42] Korobko DA, Okhotnikov OG, Stoliarov DA, Sysolyatin AA, Zolotovskii IO. Broadband infrared continuum generation in dispersion shifted tapered fiber. J Opt Soc Am B 2015;32(4):692–700. https://doi.org/10.1364/JOSAB.32.000692.
[43] Tolstik N, Sorokin E, Kalashnikov V, Klimentov D, Dvoyrin V, Sorokina IT. Supercontinuum generation in mid-IR using chalcogenide and germanate nonlinear fiber. Proc SPIE 2013;8599(March 2013):1–6. https://doi.org/10.1117/12.2003957.
[44] Efimov A, Taylor AJ, Omenetto FG, Yulin AV, Joly NY, Biancalana F, Skryabin DV, Knight JC, Russell PS. Time-spectrally-resolved ultrafast nonlinear dynamics in small-core photonic crystal fibers: Experiment and modelling. Opt Express 2004;12(26):6498–507. https://doi.org/10.1364/OPEX.12.006498.
[45] Rezvani SA, Nomura Y, Ogawa K, Fuji T. Generation and characterization of mid-infrared supercontinuum in polarization maintained zblan fibers. Opt Express 2019;27(17):24499–511. https://doi.org/10.1364/OE.27.024499.
[46] Qin G, Yan X, Kito C, Liao M, Chaudhari C, Suzuki T. Ultra-broadband supercontinuum generation from ultraviolet to 6.28 μm in a fluoride fiber. Optical Fiber Communication Conference Optical Society of America; 2010. p. 1–3. https://doi.org/10.1364/OFC.2010.OTuJ6.
[47] Nagl N, Mak KF, Wang Q, Pervak V, Krausz F, Pronin O. Efficient femtosecond mid-infrared generation based on a cr:zns oscillator and step-index fluoride fibers. Opt Lett 2019;44(10):2390–3. https://doi.org/10.1364/OL.44.002390.
[48] Møller U, Yu Y, Kubat I, Petersen CR, Gai X, Brilland L, Méchin D, Caillaud C, Troles J, Luther-Davies B, Bang O. Multi-milliwatt mid-infrared supercontinuum generation in a suspended core chalcogenide fiber. Opt Express 2015;23(3):3282–91. https://doi.org/10.1364/OE.23.003282.
[49] Korobko D, Rastogi V, Sysoliatin A, Zolotovskii I. Generation of 2 μm radiation due to single-mode fibers with longitudinally varying diameter. Opt Fiber Technol 2019;47:38–42. https://doi.org/10.1016/j.yofte.2018.11.008.
[50] Fedotov AB, Naumov AN, Zheltikov AM, Bugar I, Chorvat D, Chorvat D, Tarasevitch AP, von der Linde D. Frequency-tunable supercontinuum generation in photonic-crystal fibers by femtosecond pulses of an optical parametric amplifier. J Opt Soc Am B 2002;19(9):2156–64. https://doi.org/10.1364/JOSAB.19.002156.
[51] Beaud P, Hodel W, Zysset B, Weber H. Ultrashort pulse propagation, pulse breakup, and fundamental soliton formation in a single-mode optical fiber. IEEE J Quantum Electron 1987;23(11):1938–46. https://doi.org/10.1109/JQE.1987.1073262.
[52] Godard A. Infrared (2–12 μm) solid-state laser sources: a review. CR Phys 2007;8(10):1100–28. https://doi.org/10.1016/j.crhy.2007.09.010.
[53] Ebrahim-Zadeh M, Kumar SC, Esteban-Martin A, Samanta GK. Breakthroughs in photonics 2012: Breakthroughs in optical parametric oscillators. IEEE Photonics J 2013;5(2):10–5. https://doi.org/10.1109/JPHOT.2013.2255268.
[54] Petrov V. Parametric down-conversion devices: The coverage of the mid-infrared spectral range by solid-state laser sources. Opt Mater 2012;34(3):536–54. https://doi.org/10.1016/j.optmat.2011.03.042.
[55] Vengelis J, Tumas A, Pipinyte I, Kuliešaite M, Tamuliene V, Jarutis V, Grigonis R, Sirutkaitis V. Characteristics of optical parametric oscillator synchronously pumped by Yb:KGW laser and based on periodically poled potassium titanyl phosphate crystal. Opt Commun 2018;410:774–81. https://doi.org/10.1016/j.optcom.2017.11.057.
[56] Pipinytė I, Tamulienė V, Vengelis J, Grigonis R, Sirutkaitis V. Temporal characteristics of a synchronously pumped optical parametric oscillator at different conditions of cavity losses. J Opt Soc Am B 2019;36(10):2735–43. https://doi.org/10.1364/JOSAB.36.002735.
[57] Vengelis J, Jarutis V, Sirutkaitis V. Estimation of photonic crystal fiber dispersion by means of supercontinuum generation. Opt Lett 2017;42(9):1844–7. https://doi.org/10.1364/OL.42.001844.
[58] Blow KJ, Wood D. Theoretical description of transient stimulated raman scattering in optical fibers. IEEE J Quantum Electron. 1989;25(12):2665–73. https://doi.org/10.1109/3.40655.
[59] Couairon A, Brambilla E, Corti T, Majus D, Ramirez-Gongora O, Kolesik M. Practitioner's guide to laser pulse propagation models and simulation. Eur Phys J-Spec Top 2011;199. https://doi.org/10.1140/epjst/e2011-01503-3.
[60] Zhang H-Q, Wang P, Liu W-J, Yao Y-L, Xu Z-J, Li J. 19-fs pulse generated by supercontinuum compression. Chin Phys B 2016;25(2):024209 https://doi.org/10.1088/1674-1056/25/2/024209.
[61] Skryabin DV, Gorbach AV. Colloquium: Looking at a soliton through the prism of optical supercontinuum. Rev Mod Phys 2010;82(2):1287–99.
[62] Nishizawa N, Goto T. Characteristics of pulse trapping by use of ultrashort soliton pulses in optical fibers across the zero-dispersion wavelength. Opt Express 2002;10(21):1151–9. https://doi.org/10.1364/OE.10.001151.